AlxC Monolayer Sheets: Two-Dimensional Networks with Planar Tetracoordinate Carbon and Potential Applications as Donor Materials in Solar Cell

ARTICLE *in* JOURNAL OF PHYSICAL CHEMISTRY LETTERS · MAY 2014

Impact Factor: 7.46 · DOI: 10.1021/jz500674e

4 AUTHORS:

Jun Dai
University of Nebraska at Lincoln
41 PUBLICATIONS **609** CITATIONS
SEE PROFILE

Xiaojun Wu
University of Science and Technology of China
114 PUBLICATIONS **2,338** CITATIONS
SEE PROFILE

Jinlong Yang
University of Science and Technology of China
510 PUBLICATIONS **11,091** CITATIONS
SEE PROFILE

Zeng Cheng
University of Science and Technology of China
380 PUBLICATIONS **6,802** CITATIONS
SEE PROFILE

THE JOURNAL OF PHYSICAL CHEMISTRY Letters

Letter

pubs.acs.org/JPCL

Al_xC Monolayer Sheets: Two-Dimensional Networks with Planar Tetracoordinate Carbon and Potential Applications as Donor Materials in Solar Cell

Jun Dai,[†] Xiaojun Wu,[‡] Jinlong Yang,[§] and Xiao Cheng Zeng*[,†,§]

[†]Department of Chemistry and Department of Mechanical and Materials Engineering, University of Nebraska-Lincoln, 536 Hamilton Hall, Lincoln, Nebraska 68588, United States

[‡]CAS Key Lab of Materials for Energy Conversion, Department of Materials Science and Engineering and Hefei National Lab for Physical Science at Microscale, University of Science and Technology of China, 96 JinZhai Road, Hefei, Anhui 230026, China

[§]Department of Chemical Physics and Hefei National Lab for Physical Science at Microscale, University of Science and Technology of China, 96 JinZhai Road, Hefei, Anhui 230026, China

Supporting Information

ABSTRACT: We perform a global search of the most stable structures of 2D stoichiometric Al_xC (x = 1/3, 1, 2, and 3) monolayer sheets. In the most stable 2D planar AlC network, every carbon atom is tetracoordinated. In addition to the structure of AlC, structures of the most stable Al_2C and Al_3C monolayer sheets are also predicted for the first time. AlC and Al_2C monolayers are semiconducting, while Al_3C monolayer is metallic. In particular, Al_2C monolayer possesses a bandgap of 1.05 eV (based on HSE06 calculation), a value suitable for photovoltaic applications. Moreover, three Al_2C/WSe_2, $Al_2C/MoTe_2$, and AlC/ZnO van der Waals heterobilayers are investigated, and their power conversion efficiencies are estimated to be in the range of 12−18%. The near-perfect match in lattice constants between the Al_2C monolayer and PdO (100) surface suggests strong likelihood of experimental realization of the Al_2C monolayer on the PdO (100) substrate.

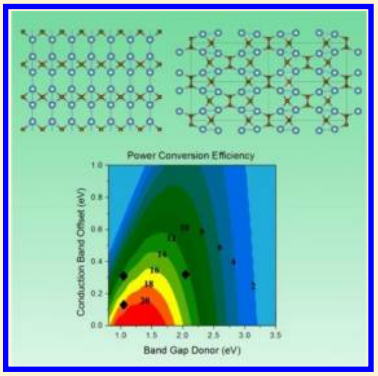

SECTION: Molecular Structure, Quantum Chemistry, and General Theory

As one of most popular elements in nature, carbon is known for its capability to form sp-, sp^2-, and sp^3-hybridized bonds. In bulk diamond and lonsdaleite, carbon exhibits tetrahedral sp^3 coordination, while in low-dimensional carbon allotropes such as graphite, 2D graphene,[1] 1D carbon nanotubes,[2,3] and 0D fullerene,[4] carbon displays sp^2 hybridization. Moreover, in 2D graphyne and graphydine monolayer sheets, carbon atoms are predicted to form both sp and sp^2 bonds.[5,6] Besides the sp, sp^2, and sp^3 hybridizations, Hoffmann et al. predicted the possible existence of planar tetracoordinate carbon (ptC).[7] This intriguing chemical bonding of carbon has attracted growing attention since 1970; considerable research efforts have been devoted to producing chemical species that contain the ptC.[8−10] To date, two possible ways are commonly considered to stabilize a ptC system: (1) incorporating substituents of strong σ-donors and π-acceptors to mitigate the lacking of σ electron density and to decrease the unstable π electron density and (2) incorporating a ptC unit into a rigid steric framework in which the steric forces can stabilize the ptC configuration. Since the first ptC compound synthesized by Cotton and Millar in 1977,[11] numerous ptC-containing molecules have been either theoretically predicted or experimentally detected.[8−10,12,13]

The successful isolation of 2D graphene in 2004 has also greatly boosted research interests in 2D monolayer materials with atomic thickness.[14] Growing attention has also been paid to 2D materials containing ptC units. For example, on the basis of the simplest ptC species C_5^{2-}, Pancharatna et al. constructed 1D, 2D, and 3D networks of stoichiometric C_5M_x (M = Li, x = 2; M = Be, Pt, Zn, x = 1).[15] Wu et al. predicted highly stable B_2C monolayer, single-walled B_2C nanotubes and nanoribbons containing ptC. This prediction was inspired from the stable molecular BC_4 motif.[16] A global search of the most stable structures of 2D B_xC_y compounds also suggests that the ptC-containing 2D networks are likely the most stable structures among the B_2C, B_3C, and B_5C monolayer sheets.[17] The $C_3B_2H_2$ ptC unit was used to construct nanoribbons and nanotubes.[18,19] Moreover, ptC was predicted to exit in transition-metal-decorated graphene ribbons[20] and transition-metal-connected graphene biwings and triwings.[21] Very recently, 2D tetragonal TiC monolayer with quasi-planar tetracoordinate carbon has been predicted by Zhang et al.[22] Regarding the Al−C systems, several extended structures with containing ptC have been predicted. For instance, on the basis of the experimentally characterized AlC_4^{2-} motif, bulk ionic materials containing

Received: April 4, 2014
Accepted: May 27, 2014
Published: May 27, 2014

   dx.doi.org/10.1021/jz500674e | J. Phys. Chem. Lett. 2014, 5, 2058−2065

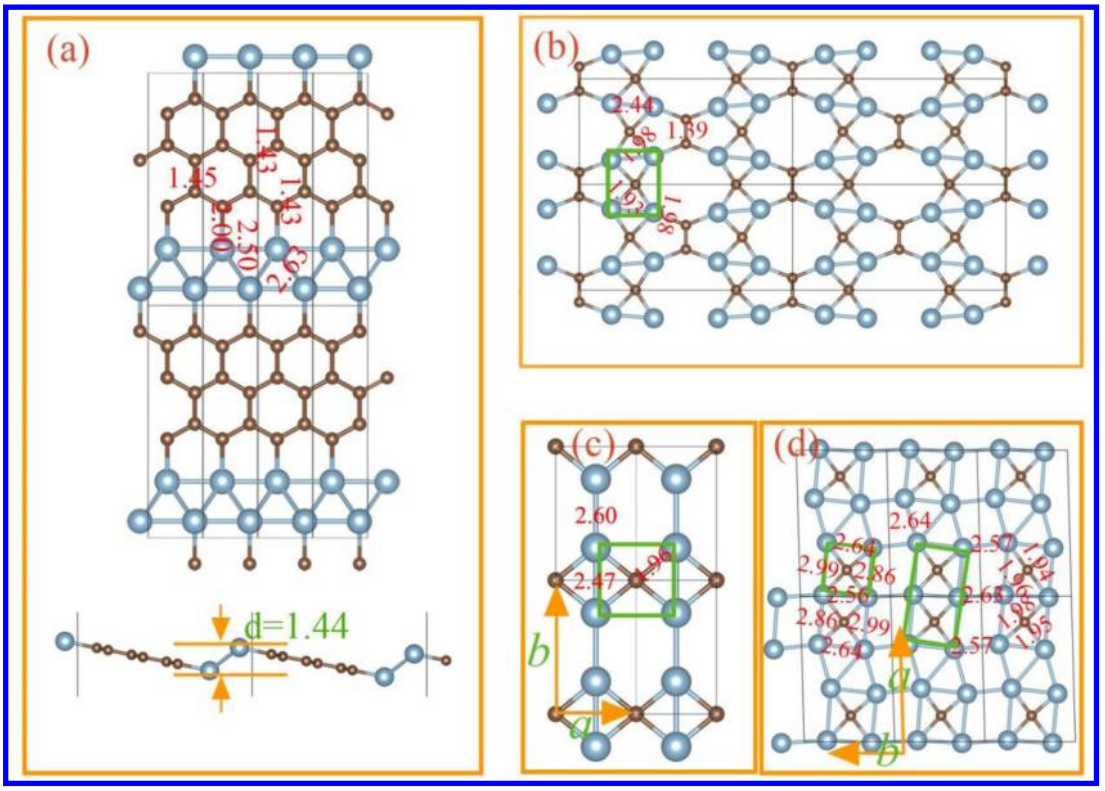

Figure 1. Predicted most stable monolayer structure of (a) AlC_3, (b) AlC, (c) Al_2C, and (d) Al_3C. To illustrate the buckled structure of AlC_3, we present both top and side views in panel a. Al and C atoms are denoted by silver and brown spheres. The ptC units are highlighted with green rectangles. The unit of the bond lengths is angstroms.

Na^+[23,24] and alkali- and alkaline-earth metal sandwich complexes have been designed.[25−28] Wu et al. constructed 1D molecular chains based on the ptC containing C_2Al_4 unit.[29] Besides ptC, ptSi-containing silagraphene[30] and 2D B−Si compounds[31] have also been predicted.

We note that the ptC-containing Al−C species are among the most studied molecular systems on the ptC chemistry.[12,23,24,29,32] However, to date, little attention has been paid to the extended 2D Al−C systems that entail the ptC chemistry. On the basis of Allen's definition,[33] the difference in electronegativity between Al and C is 0.931, close to that between B and N (1.015). Since the electronic bandgap usually increases with the difference in electronegativity for binary compounds, 2D Al−C monolayers might possess a desirable bandgap suitable for electronic or optoelectronic applications. In this work, we employ a global optimization method based on the particle-swarm optimization (PSO) algorithm[34,35] to search for the most stable structures of stoichiometric Al−C monolayers. The most stable structures of 2D AlC_3, AlC, Al_2C, and Al_3C sheets are predicted for the first time. In particular, the ptC-containing AlC, Al_2C, and Al_3C monolayers are obtained. Density functional theory (DFT) calculations with screened-hybrid HSE06[36,37] functional suggest that the AlC and Al_2C monolayers are semiconducting with a bandgap of 2.05 and 1.05 eV, respectively. Interestingly, we find that the optimized lattice constants of Al_2C monolayer (a = 3.03 Å, b = 5.06 Å) are nearly the same as those of the PdO-terminated PdO (100) surfaces (a = 3.08 Å, b = 5.46 Å), suggesting that the Al_2C monolayer may be synthesized on the PdO (100) surface (serving as a template). Furthermore, we predict that the Al_2C/WSe_2 van der Waals heterobilayer may be a potential van der Waals material for solar-cell application due to its high theoretical efficiency (∼18%) for power conversion.

The predicted most stable structures of 2D Al−C compounds with various Al−C stoichiometric compositions are listed in Figure 1. For the AlC_3 monolayer (Figure 1a), its structure can be viewed (in top view) as an alternative arrangement of zigzag graphene nanoribbons and Al nanoribbons. AlC_3 monolayer is nonplanar, and the energy of the planar AlC_3 is 0.050 eV/atom higher than the nonplanar one. In the side view (Figure 1a), the graphene nanoribbon and Al nanoribbon exhibit an interplanar angle of 132.1° with a buckled distance of 1.44 Å. In the AlC_3 monolayer, the Al−Al bond lengths are 2.50 and 2.63 Å, the Al−C bond length is 2.00 Å, and the C−C bond lengths are 1.43 and 1.45 Å, respectively.

All AlC, Al_2C, and Al_3C monolayers (Figure 1b−d) contain the ptC motif, and all three monolayers are planar. The most stable structure of AlC (Figure 1b) can be viewed as periodic and parallel $[Al_4C_2]_n$ chains connected by parallel C−C dimer chains. Each $[Al_4C_2]_n$ chain is composed of connected Al_4C units where each carbon atom is bonded with four Al atoms, forming a ptC motif. Each C−C dimer together with the four neighboring Al atoms and two carbon atom forms two neighboring Al_2C_3 pentagons. Between two neighboring $[Al_4C_2]_n$ chains, the Al_4C_4 octagons give rise to an "8558" line defect. The closest Al−Al distance in AlC is 2.44 Å, the bond length of C−C dimer is 1.39 Å, and the Al−C bond lengths in the ptC are 1.93 and 1.98 Å, respectively.

The Al_2C monolayer has a similar structure as previously predicted structure of B_2C−IV[16,17] or SiC_2.[30] The optimized lattice constants for the Al_2C monolayer, labeled as a and b in Figure 1c, are a = 3.04 Å and b = 5.07 Å, respectively. The Al_2C monolayer can be viewed as fused Al_4C units, as highlighted by

dx.doi.org/10.1021/jz500674e | J. Phys. Chem. Lett. 2014, 5, 2058−2065

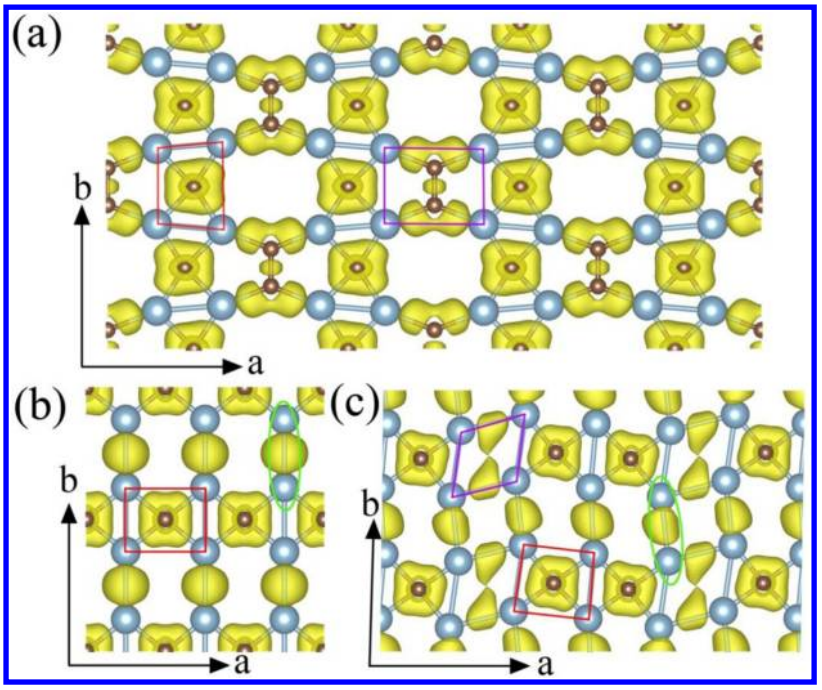

Figure 2. Isosurfaces of ELF with the value of 0.75 for (a) AlC, (b) Al_2C, and (c) Al_3C.

a green rectangle in Figure 1c. Along the *a* direction, two neighboring Al_4C units share a pair of Al atoms, while along the *b* direction, the two neighboring Al_4C units are connected via two Al−Al bonds with the Al−Al bond length of 2.60 Å. The Al−C bond length in each Al_4C unit is 1.96 Å, and the Al−Al distance along the *b* direction is 2.47 Å.

The Al_3C monolayer can be viewed as a 2D network of Al_6C_2 units. An Al_6C_2 unit is composed of two edge-sharing Al_4C units. As shown in Figure 1d, along the *a* direction, Al_6C_2 units are connected via two Al−Al bonds, and along the *b* direction, Al_6C_2 units are connected with three Al−Al bonds. Note that the two Al_4C units in Al_6C_2 are slightly distorted, where the Al−C bond lengths are within the range of 1.94 to 1.98 Å, the Al−Al bond lengths are 2.56 and 2.64 Å along the *b* direction, and 2.86 and 2.99 Å are along the *a* direction, respectively. The Al−Al bond lengths between two adjacent Al_6C_2 units are 2.64 Å along the *a* direction and 2.57 and 2.63 Å along the *b* direction, respectively.

To better understand bonding nature of the predicted ptC-containing AlC, Al_2C, and Al_3C monolayers, we undertake an analysis of electron localization function (ELF).[38,39] For highlighting the in-plane σ states, we plot isosurface of ELFs for AlC, Al_2C, and Al_3C monolayers, all with an isovalue of 0.75 au, as shown in Figure 2. The AlC monolayer exhibits two ELF domains: One is the ptC containing Al_4C (highlighted by a red quadrangle in Figure 2a), where ELF distributes around the C-centered four Al−C bonds, while another is the C−C dimer containing Al_4C_2 (highlighted by a purple quadrangle in Figure 2a), where one C−C σ bond and four Al−C σ bonds are seen. The bonding between Al−Al in the AlC monolayer is weak. For Al_2C, the ELF distributes symmetrically around the ptC, the Al−Al bonding in the ptC-containing Al_4C domain (see the red rectangle in Figure 2b) is weak, while the Al atoms between the two neighboring Al_4C along the *b* direction form Al−Al σ bonds (see area highlighted by green long oval in Figure 2b). For Al_3C, we can see that along the *b* direction, the Al atoms between two edge-sharing Al_6C_2 units form Al−Al σ bonds, and along the *a* direction, ELF is mainly distributed along the Al−Al bonds in the *a* direction for the four Al atoms between the two neighboring Al_6C_2 units (highlighted by purple quadrangle in Figure 2c).

To examine structure stabilities of the four 2D stoichiometric Al−C monolayers, we computed cohesive energies of these compounds. The computed cohesive energies of AlC_3, AlC, Al_2C, and Al_3C monolayers are 6.46, 5.17, 4.45, and 3.97 eV/atom, respectively, while the computed cohesive energy of bulk Al_4C_3 is 5.53 eV/atom. The relatively large cohesive energies of new 2D Al−C compounds suggest that the monolayers are stable phases of Al−C systems. Next, we compute molar formation energy δG for Al_xC_{1-x} using the formula $\delta G(x) = -E_{coh}(x) - x\mu_{Al} - (1-x)\mu_C$, where $E_{coh}(x)$ is the cohesive energy of Al_xC_{1-x} and μ_{Al} and μ_C are chemical potentials of pure Al and C.[22,40−42] Note that μ_{Al} and μ_C represent environmental conditions and thereby a better description of relative stabilities of the 2D Al−C compounds. Relative stabilities can be determined based on the altitude of each $-E_{coh}$ point from the line connecting the reference μ_{Al} and μ_C values at $x = 0$ and $x = 1$. A phase with higher $\delta G(x)$ would be less stable. In general, a phase with its $-E_{coh}$ in the light-blue area of Figure 3 is thermodynamically stable, while the one in the light-yellow region is metastable or unstable. Here we choose μ_{Al} as $\mu_{Al} = \mu_{Al}^{bulk} = -E_{coh}(Al)$ in fcc bulk phase of Al and μ_C as that in graphene $\mu_C = \mu_C^{graphene} = -E_{coh}(C)$. As shown in Figure 3, the bulk Al_4C_3 is thermodynamically stable because its $-E_{coh}$ is below the straight line ($\delta G(4/7) = -0.10$ eV), while all predicted 2D Al−C compounds are located above the line with a positive $\delta G(x)$ value and are thus metastable. The AlC_3 (with $\delta G(1/4) = 0.40$ eV) appears to be more stable than AlC ($\delta G(x1/2) = 0.58$ eV), Al_2C ($\delta G(2/3) = 0.56$ eV), and Al_3C ($\delta G(3/4) = 0.67$ eV).

The dynamical stability of the four 2D Al−C monolayers is also confirmed via phonon spectrum calculations based on density functional perturbation theory as implemented in Quantum-Espresso package.[43] As shown in Figure S1 in the

dx.doi.org/10.1021/jz500674e | J. Phys. Chem. Lett. 2014, 5, 2058−2065

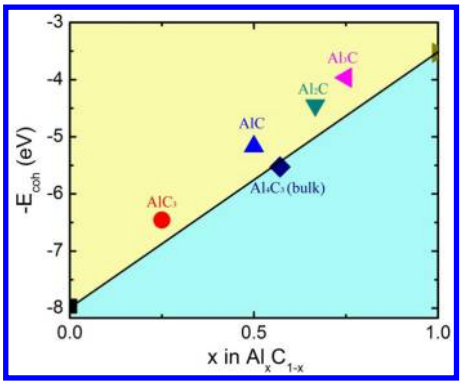

Figure 3. Cohesive energy E_{coh} for the 2D binary phases of Al_xC_{1-x} at different Al mole fraction x. The straight line connects the cohesive energies of graphene at $x = 0$ and bulk Al at $x = 1$.

Supporting Information, the phonon spectra show no imaginary phonon modes, suggesting that the monolayers are locally stable without any dynamical instability. The highest frequency is 1491 cm^{-1} for AlC_3 and 1285 cm^{-1} for AlC, significantly higher than those for Al_2C and Al_3C (896 cm^{-1} for Al_2C and 827 cm^{-1} for Al_3C). This behavior is due to the C−C bonds in AlC_3 and AlC, while in Al_2C and Al_3C, the strongest bond is Al−C bond. Although the phonon instability is the necessary and sufficient condition for testing mechanical instability of a crystal at low temperature, the thermal stability at elevated temperatures is also another important indicator for testing structure stability. To this end, a Born−Oppenheimer molecular dynamics (BOMD) simulation at DFT level is carried out for each new 2D Al−C compound. The constant-volume and constant-temperature ensemble (*NVT*) is adopted. The initial structures for the BOMD simulation are taken from the optimized structures at zero temperature. BOMD simulations are performed with temperature controlled at 1000, 2000, and 2500 K, respectively, for all AlC_3, AlC, and Al_2C monolayers and at 1000, 1500, and 2000 K for Al_3C. Snapshots at 9 ps of the simulation are plotted for each system at each given temperature. (See Figure S2 in the Supporting Information.) It can be seen that AlC_3, AlC, and Al_2C are likely to melt at a temperature between 2000 and 2500 K, while for Al_3C, the melting temperature is between 1500 and 2000 K. These results indicate that the predicted 2D Al−C compounds can be thermally stable under high-temperature environment.

Elastic constants of the ptC-containing AlC, Al_2C, and Al_3C monolayers are computed and listed in Table 1. As a benchmark, the elastic constants of graphene are also computed at the same level of DFT, which are C_{11} = 1005.6 GPa, C_{12} = 180 GPa, and C_{66} = 412.8 GPa, in good agreement with experimental results (C_{11} = 1060 GPa, C_{12} = 180 GPa, C_{66} = 440 GPa).[44] Our results show that the C_{ij} constants of AlC, Al_2C, and Al_3C are lower than those of the graphene, consistent with the fact that the in-plane bonding of these predicted structures are weaker than that of graphene. Taking AlC as an example (see Figure 2a), the Al−C- and C-centered regions are weaker than the C−C σ bonding in graphene. Nevertheless, several C_{ij} constants of AlC, Al_2C, and Al_3C are higher than reported values for SiC (C_{11} = 118.8 GPa, C_{12} = 255.5 GPa), Si_2C (C_{11} = 143.0 GPa, C_{12} = 41.4 GPa, C_{22} = 142.3 GPa), and silicene (C_{11} = 287 GPa, C_{12} = 127 GPa) monolayers,[45] while those of Al_3C and silicene are comparable to one another. Hence, the ptC-containing Al−C monolayers possess relatively good elastic property.

Table 1. Calculated Elastic Constants of AlC, Al_2C, and Al_3C Monolayer Sheets in Gigapascals

	C_{11}	C_{22}	C_{12}	C_{66}
AlC	395.8	333.1	74.0	109.3
Al_2C	344.8	315.2	35.9	61.0
Al_3C	239.0	242.4	38.0	30.2
graphene	1005.6	= C_{11}	180	412.8

The electronic band structures, together with atomic and orbital projected density of states (PDOS), are plotted in Figure 4. The metallic feature of AlC_3 and Al_3C monolayers is expected because one can see fully connected carbon and aluminum chains in AlC_3 and fully connected aluminum chains in Al_3C. For AlC_3, the electronic states near the Fermi level are mainly contributed by carbon's delocalized $2p_z$ π electrons, where π and π^* bands intersect at S point, showing a metallic feature. For Al_3C, as shown in Figure 4d, it has two bands across the Fermi level, and both aluminum's s and p electrons and carbon's p_z electrons contribute to the states near the Fermi level.

The AlC monolayer has a bandgap of 1.26 eV, and both valence band maximum (VBM) and the conduction band minimum (CBM) are located at the Γ point, a feature of direct-gap semiconductor. Electronic orbital analysis indicates that the VBM is from the p_z states of the pt-C atoms, while the CBM is from the mixed p_z states of C atoms in C−C dimers and their neighboring Al atoms. (See Figure S3 of the Supporting Information).

The Al_2C monolayer is a semiconductor with an indirect bandgap of 0.47 eV. Its VBM at S is from the p_z states of carbon, and the CBM at Y is from the p_z states of Al. (See Figure S4 of the Supporting Information.) Interestingly, the top of the valence band at Y also stems from Al p_z states, and the direct bandgap at Y is 0.56 eV, close to the indirect gap of 0.47 eV. For both AlC and Al_2C monolayers, the in-plane bonding σ states are fully occupied and the antibonding σ^* states are empty. This feature that the Fermi level is located within the gap of the in-plane PDOS, that is, the in-plane bonding σ states are fully occupied, the antibonding σ^* states are unfilled, while the remaining electrons either fill or partially fill the out-of-plane π states, has been used to explain the peculiar stability of boron monolayers,[46−48] 2D boron−carbon compounds,[17] or 2D boron−silicon compounds.[31] A reason why the most stable structures of these 2D materials can be understood by the optimal filling of the in-plane states is that the in-plane σ bonds are stronger than the out-of-plane π bonds. This feature is also consistent with the stability analysis based on the molar formation energy and BOMD simulations; namely, the AlC and Al_2C monolayers have lower δG values and higher melting points than Al_3C.

It is known that the PBE functional tends to underestimate the bandgap of semiconductors and may give an incorrect gap feature for some narrow-gap semiconductors. Additional computation of the electronic band structures is carried out based on the screened HSE06 hybrid functional,[36,37] which has been shown to give more reliable bandgaps for many semiconductors, including diamond and AlN.[49] As shown in Supporting Information Figure S5, HSE06 band structures show qualitatively the same features as those based on PBE functional, that is, the metallic features of AlC_3 and Al_3C, the direct-gap semiconducting feature of AlC, and the indirect-gap

dx.doi.org/10.1021/jz500674e | J. Phys. Chem. Lett. 2014, 5, 2058−2065

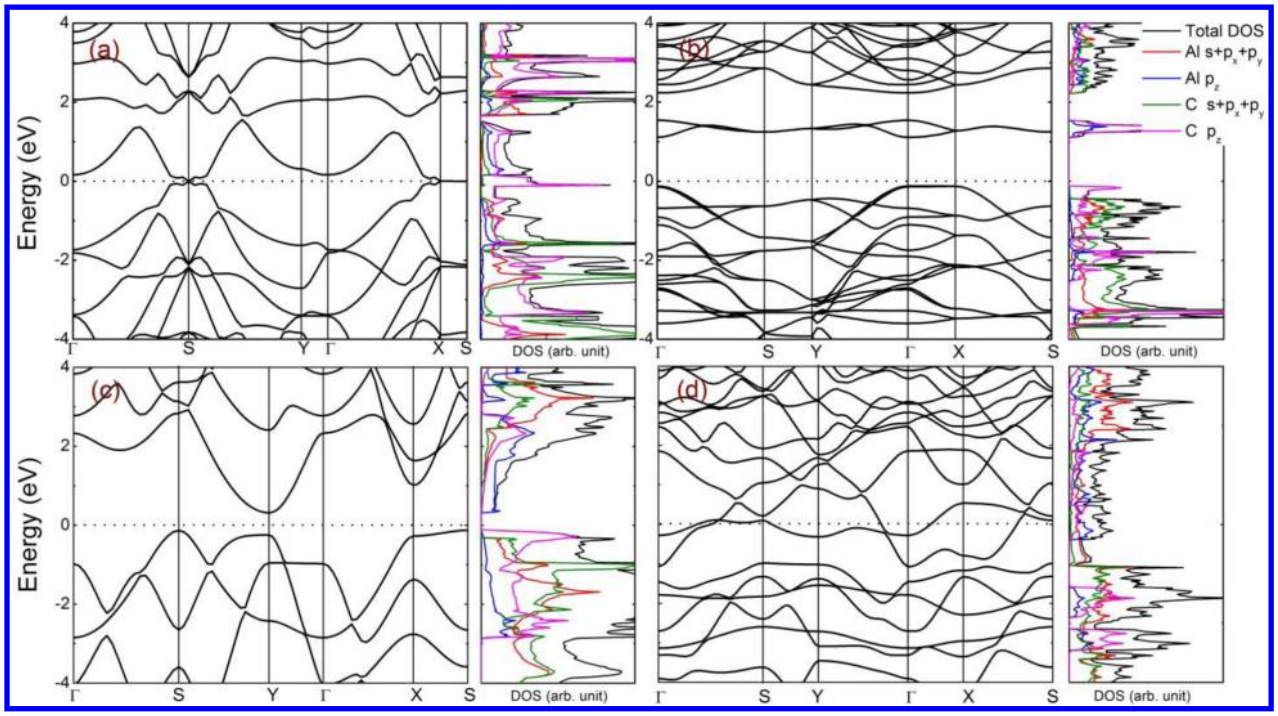

Figure 4. Computed electronic band structures and projected density of states (pDOS) based on PBE functional of (a) AlC_3, (b) AlC, (c) Al_2C, and (d) Al_3C. The Fermi level is set to zero.

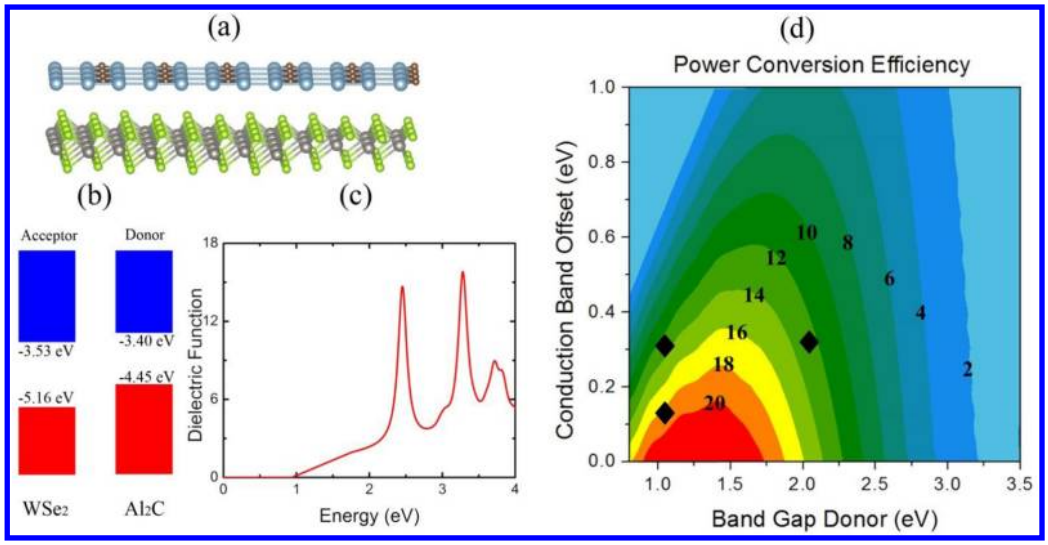

Figure 5. (a) Schematic drawing of an interface between Al_2C and WSe_2 monolayers. (b) Band offsets between Al_2C and WSe_2 monolayers. (c) Computed imaginary part of the frequency-dependent dielectric function. (d) Power conversion efficiency as a function of the donor bandgap and conduction band offset.

semiconducting feature of Al_2C, suggesting that the PBE calculation is qualitatively reliable for the Al−C systems. The bandgaps predicted via HSE06 calculation are 2.05 eV for AlC, 1.05 eV (indirect Y−S), and 1.25 eV (direct Y−Y) for Al_2C, respectively. The direct bandgap of AlC renders the material a promising candidate for optoelectronic applications. Note that the predicted bandgap of Al_2C is very close to that of bulk Si (PBE 0.58 eV, HSE06 1.15 eV, experimental 1.12 eV).[50] Such similarity in bandgap between Al_2C monolayer with bulk Si points out a possibility of using 2D Al−C materials in future as complementary metal-oxide semiconductor (CMOS) devices.

Our HSE06 calculations indicate that the Al_2C monolayer possesses similar electronic structures as bulk Si, and the AlC monolayer has a direct bandgap of 2.05 eV. These results suggest that both monolayers may be applied as solar cell donor materials if an appropriate acceptor material can be found. For the Al_2C monolayer, the computed VBM and CBM levels (HSE06) are −4.45 and −3.40 eV, respectively, while for the WSe_2 monolayer, the computed VBM and CBM levels are −5.16 and −3.53 eV, respectively. The latter levels match those of Al_2C monolayer very well, giving a type-II alignment with both materials. (See Figure 5b.) Thus, a potential solar-cell device made of Al_2C and WSe_2 monolayers is constructed, as shown in Figure 5a. The computed imaginary part of the frequency-dependent dielectric function of Al_2C, based on GW-BSE approach, is plotted in Figure 5c. We can see that the

dx.doi.org/10.1021/jz500674e | J. Phys. Chem. Lett. 2014, 5, 2058−2065

optical absorption is fairly strong over a wide energy range between 2 and 4 eV, a range important for enhancing efficiency of a solar cell. Similar devices could be constructed with Al_2C/$MoTe_2$ or AlC/ZnO bilayer, in which the CBM of $MoTe_2$, AlC, and ZnO is −3.71, −2.51, and −2.83 eV, respectively, and the corresponding VBM is −4.99, −4.56, and −6.12 eV, respectively. The upper limit of the power conversion efficiency (PCE) η is estimated in the limit of 100% external quantum efficiency (EQE),[51,52] $\eta = J_{sc}V_{oc}\beta_{FF}/P_{solar} = 0.65(E_g^d - \Delta E_c - 0.3)\int_{E_g}^{\infty}(P(\hbar\bar{\omega}))/\hbar\bar{\omega})\ d(\hbar\bar{\omega})/\int_0^{\infty}P(\hbar\bar{\omega})d(\hbar\bar{\omega})$, where the fill factor (FF) is taken to be 0.65, $P(\hbar\bar{\omega})$ is the AM1.5 solar energy flux (expressed in $Wm^{-2}eV^{-1}$) at the photon energy $\hbar\bar{\omega}$, E_g^d is the bandgap of the donor material, ΔE_c is the offset of conduction bands, $d(\hbar\bar{\omega})$ indicates integration over $\hbar\bar{\omega}$, the $(E_g^d - \Delta E_c - 0.3)$ term is an estimation of the maximum open-circuit voltage V_{oc}, and 0.3 eV is an empirical value for the efficient electron−hole charge separation. The integral in the numerator is the short-circuit current J_{sc} in the limit of 100% EQE, and the integral in the denominator is the integrated AM1.5 solar flux. As shown in Figure 5d, the Al_2C/WSe_2, Al_2C/$MoTe_2$, and AlC/ZnO heterobilayers could yield PCE of 18.4, 13.0, and 12.6%, respectively. These PCE values are comparable to those of the PCBM/CBN system (10−20%)[51] as well as recently predicted g-SiC_2-based systems (12−20%)[45] and bilayer phosphorene/MoS_2 system (16−18%).[53]

Although the newly predicted 2D Al−C monolayers show intriguing structural and electronic properties for potential applications in solar cells, how to synthesize these materials is a critical issue. Remarkably, we find that the lattice constants of the Al_2C monolayer match those of PdO-terminated PdO(100) surface very well. Our PBE calculations show that the optimized lattice constants of Al_2C are a = 3.03 Å, b = 5.07 Å and those for PdO (100) surface are a = 3.08 Å, b = 5.46 Å. Moreover, the total energy of Al_2C with lattice parameter a = 3.08 Å and b = 5.46 Å is only 0.089 eV/atom higher than that of Al_2C with the optimized lattice parameter. Note also that the PdO-terminated (100) surface is predicted to be the most stable surface termination among all of 1 × 1 low-index surfaces.[54] Thus, we propose to synthesize the Al_2C monolayer on PdO (100) surface using prevailing techniques such as CVD or MBE. (See Figure S6 in the Supporting Information for a schematic view.)

In conclusion, we have performed a global search of the most stable monolayer structures of Al_xC compounds with x = 0.5, 1, 2, and 3. Our DFT calculations predicted three stable planar Al−C monolayers, namely, AlC, Al_2C, and Al_3C sheets, which all contain the planar tetracoordinate carbon. In particular, the AlC and Al_2C monolayers are predicted to be semiconducting. Al_2C has a bandgap of 1.05 eV, comparable to that of bulk Si. More importantly, we predict that the Al_2C/WSe_2, Al_2C/$MoTe_2$, and AlC/ZnO van der Waals heterobilayers can be promising for solar-cell applications due to their type-II alignment. The theoretical upper limit of PCE for these heterobilayers is in the range of 12−18%. Finally, we propose that the Al_2C monolayer can be synthesized on the PdO (100) surface due to the remarkable lattice-constant match between the Al_2C monolayer and PdO (100) surface.

COMPUTATIONAL METHODS

PSO Structural Search. The structure search is performed using the PSO algorithm within the revolutionary scheme, as implemented in the CALYPSO (Crystal structure AnaLYsis by Particle Swarm Optimization) code.[34,35] The PSO algorithm offers an efficient and fast way to obtain reliable structures with only the input of chemical composition. It also requires very few parameters to adjust. In combination with DFT optimization, the PSO algorithm has been shown to successfully predict low-energy structures of 2D boron−carbon compounds,[17] boron monolayer sheets,[48] 2D boron−silicon compounds,[31] SiC_2 siligraphene,[45] and numerous 3D ground-state structures of elements and compounds.[55−61] For the Al−C systems, we consider four Al/C ratios for the structure search, including AlC_3, AlC, AlC_2, and AlC_3. Specifically, in the PSO search, the population size is set to be 30, and the number of generations is maintained at 30. Various supercell sizes are considered with the total number of atoms less than 16 in the supercell. Taking AlC as an example, supercell sizes up to eight unit cells have been examined. As such, a total number of 7200 configurations are probed to ensure the unbiased search. In the first generation of the structure search, random structures are constructed by generating atomic coordinates using crystallographic symmetry operations. These structures are then optimized by using a DFT method. The best 60% structures are selected through PSO to generate the next generation, while the other structures are generated randomly to guarantee the structure diversity.

DFT Calculations. The electronic band structures are computed using DFT methods implemented in VASP package.[62,63] The DFT calculations are within the framework of generalized gradient approximation (GGA) in the form of Perdew−Burke−Ernzerhof (PBE) for the exchange-correlation energy. The ion−electron interaction is treated using the projecter-augmented wave (PAW) method.[64] For geometric optimization, both lattice constants and atomic positions are relaxed until the forces on atoms are <0.02 eV/Å, and the total energy change is $<1.0 \times 10^{-5}$ eV. A vacuum distance of ∼20 Å is adopted so that the interlayer interaction is negligible. For the geometric optimization, the Brillouin zone is sampled using k points with 0.02 $Å^{-1}$ spacing in the Monkhorst−Pack scheme,[65] while for computing the density of states and total energies a denser k-point grid with 0.01 $Å^{-1}$ spacing is used.

ASSOCIATED CONTENT

Supporting Information

Phonon band structures of AlC_3, AlC, Al_2C, and Al_3C monolayer sheets, BOMD snapshots of AlC_3, AlC, Al_2C, and Al_3C monolayer sheets at different temperatures, isosurface plots of VBM and CBM for AlC and Al_2C monolayer sheets, HSE06 band structures for AlC_3, AlC, Al_2C, and Al_3C monolayer sheets, schematic view of Al_2C on PdO (100) surface, and details of HSE06 and GW/BSE computation. This material is available free of charge via the Internet at http://pubs.acs.org.

AUTHOR INFORMATION

Corresponding Author

*E-mail: xzeng1@unl.edu.

Notes

The authors declare no competing financial interest.

ACKNOWLEDGMENTS

The USTC group is supported by the National Basic Research Programs of China (nos. 2011CB921400, 2012CB 922001), NSFC (grant nos. 21121003, 51172223), One Hundred Person Project of CAS, Strategic Priority Research Program of CAS

(XDB01020300), Fundamental Research Funds for the Central Universities (WK2060140014, WK2060190025), Shanghai Supercomputer Center, and Hefei Supercomputer Center. The UNL group is supported by UNL Nebraska Center for Energy Sciences Research, ARL (grant no. W911NF1020099), and Holland Computing Center and a grant from USTC for (1000 Talents Plan) Qianren-B summer research.

REFERENCES

(1) Novoselov, K. S.; Geim, A. K.; Morozov, S.; Jiang, D.; Zhang, Y.; Dubonos, S.; Grigorieva, I.; Firsov, A. Electric Field Effect in Atomically Thin Carbon Films. *Science* **2004**, *306*, 666−669.
(2) Iijima, S.; Ichihashi, T. Single-Shell Carbon Nanotubes of 1-nm Diameter. *Nature* **1993**, *363*, 603−605.
(3) Iijima, S. Helical Microtubules of Graphitic Carbon. *Nature* **1991**, *354*, 56−58.
(4) Kroto, H. W.; Heath, J. R.; O'Brien, S. C.; Curl, R. F.; Smalley, R. E. C 60: Buckminsterfullerene. *Nature* **1985**, *318* (6042), 162−163.
(5) Baughman, R.; Eckhardt, H.; Kertesz, M. Structure-property Predictions for New Planar Forms of Carbon: Layered Phases Containing sp^2 and sp Atoms. *J. Chem. Phys.* **1987**, *87*, 6687.
(6) Narita, N.; Nagai, S.; Suzuki, S.; Nakao, K. Optimized Geometries and Electronic Structures of Graphyne and Its Family. *Phys. Rev. B* **1998**, *58*, 11009.
(7) Hoffmann, R.; Alder, R. W.; Wilcox, C. F., Jr. Planar Tetracoordinate Carbon. *J. Am. Chem. Soc.* **1970**, *92*, 4992−4993.
(8) Siebert, W.; Gunale, A. Compounds Containing a Planar-Tetracoordinate Carbon Atom as Analogues of Planar Methane. *Chem. Soc. Rev.* **1999**, *28*, 367−371.
(9) Keese, R. Carbon Flatland: Planar Tetracoordinate Carbon and Fenestranes. *Chem. Rev.* **2006**, *106*, 4787−4808.
(10) Merino, G.; Méndez-Rojas, M. A.; Vela, A.; Heine, T. Recent Advances in Planar Tetracoordinate Carbon Chemistry. *J. Comput. Chem.* **2007**, *28*, 362−372.
(11) Cotton, F. A.; Millar, M. The Probable Existence of a Triple Bond Between Two Vanadium Atoms. *J. Am. Chem. Soc.* **1977**, *99*, 7886−7891.
(12) Li, X.; Wang, L.-S.; Boldyrev, A. I.; Simons, J. Tetracoordinated Planar Carbon in the Al4C-anion. A Combined Photoelectron Spectroscopy and Ab Initio Study. *J. Am. Chem. Soc.* **1999**, *121*, 6033−6038.
(13) Wang, L.-S.; Boldyrev, A. I.; Li, X.; Simons, J. Experimental Observation of Pentaatomic Tetracoordinate Planar Carbon-Containing Molecules. *J. Am. Chem. Soc.* **2000**, *122*, 7681−7687.
(14) Butler, S. Z.; Hollen, S. M.; Cao, L.; Cui, Y.; Gupta, J. A.; Gutiérrez, H. R.; Heinz, T. F.; Hong, S. S.; Huang, J.; Ismach, A. F.; et al. Progress, Challenges, and Opportunities in Two-Dimensional Materials Beyond Graphene. *ACS Nano* **2013**, *7*, 2898−2926.
(15) Pancharatna, P. D.; Méndez-Rojas, M. A.; Merino, G.; Vela, A.; Hoffmann, R. Planar Tetracoordinate Carbon in Extended Systems. *J. Am. Chem. Soc.* **2004**, *126*, 15309−15315.
(16) Wu, X.; Pei, Y.; Zeng, X. C. B_2C Graphene, Nanotubes, and Nanoribbons. *Nano Lett.* **2009**, *9*, 1577−1582.
(17) Luo, X.; Yang, J.; Liu, H.; Wu, X.; Wang, Y.; Ma, Y.; Wei, S.-H.; Gong, X.; Xiang, H. Predicting Two-Dimensional Boron−Carbon Compounds by the Global Optimization Method. *J. Am. Chem. Soc.* **2011**, *133*, 16285−16290.
(18) Sun, W.; Zhang, C.; Cao, Z. Novel Beltlike and Tubular Structures of Boron and Carbon Clusters Containing the Planar Tetracoordinate Carbon: A Theoretical Study of $(C_3B_2)_nH_4$ (n= 2−6) and $(C_3B_2)_n$ (n= 4−8). *J. Phys. Chem. C* **2008**, *112*, 351−357.
(19) Zhang, C.; Sun, W.; Cao, Z. Zigzag Boron− Carbon Nanotubes with Quasi-planar Tetracoordinate Carbons. *J. Am. Chem. Soc.* **2008**, *130*, 5638−5639.
(20) Wu, M.; Pei, Y.; Zeng, X. C. Planar Tetracoordinate Carbon Strips in Edge Decorated Graphene Nanoribbon. *J. Am. Chem. Soc.* **2010**, *132*, 5554−5555.
(21) Wu, M.; Pei, Y.; Dai, J.; Li, H.; Zeng, X. C. Tri-Wing Graphene Nano-Paddle-Wheel with a Single-File Metal Joint: Formation of Multi-Planar Tetracoordinated-Carbon (ptC) Strips. *J. Phys. Chem. C* **2012**, *116*, 11378−11385.
(22) Zhang, Z.; Liu, X.; Yakobson, B. I.; Guo, W. Two-Dimensional Tetragonal TiC Monolayer Sheet and Nanoribbons. *J. Am. Chem. Soc.* **2012**, *134*, 19326−19329.
(23) Li, X.; Zhang, H. F.; Wang, L. S.; Geske, G. D.; Boldyrev, A. I. Pentaatomic Tetracoordinate Planar Carbon,$[CAl_4]^{2-}$: A New Structural Unit and Its Salt Complexes. *Angew. Chem.* **2000**, *112*, 3776−3778.
(24) Geske, G. D.; Boldyrev, A. I. Ab Initio Structure of the $(Na_2[CAl_4])_2$ Dimer. Next Step Toward Solid Materials Containing Tetracoordinate Planar Carbon. *Inorg. Chem.* **2002**, *41*, 2795−2798.
(25) Yang, L.-m.; Ding, Y.-h.; Sun, C.-c. Design of Sandwichlike Complexes Based on the Planar Tetracoordinate Carbon Unit CAl_4^{2-}. *J. Am. Chem. Soc.* **2007**, *129*, 658−665.
(26) Yang, L.-m.; Ding, Y.-h.; Sun, C.-c. Assembly and Stabilization of a Planar Tetracoordinated Carbon Radical CAl_3Si: A Way to Design Spin-Based Molecular Materials. *J. Am. Chem. Soc.* **2007**, *129*, 1900−1901.
(27) Yang, L.-m.; Ding, Y.-h.; Tian, W. Q.; Sun, C.-c. Planar Carbon Radical's Assembly and Stabilization, A Way to Design Spin-Based Molecular Materials. *Phys. Chem. Chem. Phys.* **2007**, *9*, 5304−5314.
(28) Yang, L.-M.; Ding, Y.-H.; Sun, C.-C. The Si-doped Planar Tetracoordinate Carbon (ptC) Unit CAl_3Si^- Could Be Used As a Building Block or Inorganic Ligand During Cluster-Assembly. *Theor. Chem. Acc.* **2008**, *119*, 335−342.
(29) Wu, Y.-B.; Li, Z.-X.; Pu, X.-H.; Wang, Z.-X. Design of Molecular Chains Based on the Planar Tetracoordinate Carbon Unit C_2Al_4. *J. Phys. Chem. C* **2011**, *115*, 13187−13192.
(30) Li, Y.; Li, F.; Zhou, Z.; Chen, Z. SiC_2 Silagraphene and Its One-Dimensional Derivatives: Where Planar Tetracoordinate Silicon Happens. *J. Am. Chem. Soc.* **2010**, *133*, 900−908.
(31) Dai, J.; Zhao, Y.; Wu, X.; Yang, J.; Zeng, X. C. Exploration of Structures of Two-Dimensional Boron−Silicon Compounds with sp^2 Silicon. *J. Phys. Chem. Lett.* **2013**, *4*, 561−567.
(32) Wu, Y. B.; Jiang, J. L.; Lu, H. G.; Wang, Z. X.; Perez-Peralta, N.; Islas, R.; Contreras, M.; Merino, G.; Wu, J. I.; von Rague Schleyer, P. Starlike Aluminum−Carbon Aromatic Species. *Chem.—Eur. J.* **2011**, *17*, 714−719.
(33) Allen, L. C. Electronegativity Is the Average One-Electron Energy of the Valence-Shell Electrons in Ground-State Free Atoms. *J. Am. Chem. Soc.* **1989**, *111*, 9003−9014.
(34) Wang, Y.; Lv, J.; Zhu, L.; Ma, Y. Crystal Structure Prediction via Particle-Swarm Optimization. *Phys. Rev. B* **2010**, *82*, 094116-1−094116-8.
(35) Wang, Y.; Lv, J.; Zhu, L.; Ma, Y. CALYPSO: A Method for Crystal Structure Prediction. *Comput. Phys. Commun.* **2012**, *183*, 2063−2070.
(36) Heyd, J.; Scuseria, G. E.; Ernzerhof, M. Hybrid Functionals Based on a Screened Coulomb Potential. *J. Chem. Phys.* **2003**, *118*, 8207−8215.
(37) Heyd, J.; Scuseria, G. E.; Ernzerhof, M. Erratum: "Hybrid Functionals Based on a Screened Coulomb Potential" [J. Chem. Phys. 118, 8207 (2003)]. *J. Chem. Phys.* **2006**, *124*, 219906-1.
(38) Silvi, B.; Savin, A. Classification of Chemical Bonds Based on Topological Analysis of Electron Localization Functions. *Nature* **1994**, *371*, 683−686.
(39) Savin, A.; Nesper, R.; Wengert, S.; Fässler, T. F. ELF: The Electron Localization Function. *Angew. Chem. Int. Ed.* **1997**, *36*, 1808−1832.
(40) Dumitrică, T.; Hua, M.; Yakobson, B. I. Endohedral Silicon Nanotubes as Thinnest Silicide Wires. *Phys. Rev. B* **2004**, *70*, 241303-1−241303-4.
(41) Zhang, Z.; Guo, W.; Dai, Y. Freestanding (3, 0) Boron Nitride Nanotube: Expected to Be Stable Well Over Room Temperature. *Appl. Phys. Lett.* **2008**, *93*, 223108-1−223108-3.

(42) Zhang, Z.; Guo, W.; Dai, Y. Stability and Electronic Properties of Small Boron Nitride Nanotubes. *J. Appl. Phys.* **2009**, *105*, 084312-1−084312-8.
(43) Giannozzi, P.; Baroni, S.; Bonini, N.; Calandra, M.; Car, R.; Cavazzoni, C.; Ceresoli, D.; Chiarotti, G. L.; Cococcioni, M.; Dabo, I.; et al. QUANTUM ESPRESSO: A Modular and Open-source Software Project for Quantum Simulations of Materials. *J. Phys.: Condens. Matter* **2009**, *21*, 395502-1−395502-19.
(44) Blakslee, O.; Proctor, D.; Seldin, E.; Spence, G.; Weng, T. Elastic Constants of Compression-Annealed Pyrolytic Graphite. *J. Appl. Phys.* **1970**, *41*, 3373−3382.
(45) Zhou, L.-J.; Zhang, Y.-F.; Wu, L.-M. SiC2 Siligraphene and Nanotubes: Novel Donor Materials in Excitonic Solar Cell. *Nano Lett.* **2013**, *13*, 5431−5436.
(46) Tang, H.; Ismail-Beigi, S. Novel Precursors for Boron Nanotubes: The Competition of Two-Center and Three-Center Bonding in Boron Sheets. *Phys. Rev. Lett.* **2007**, *99*, 115501-1−115501-4.
(47) Penev, E. S.; Bhowmick, S.; Sadrzadeh, A.; Yakobson, B. I. Polymorphism of Two-Dimensional Boron. *Nano Lett.* **2012**, *12*, 2441−2445.
(48) Wu, X.; Dai, J.; Zhao, Y.; Zhuo, Z.; Yang, J.; Zeng, X. C. Two-Dimensional Boron Monolayer Sheets. *ACS Nano* **2012**, *6*, 7443−7453.
(49) Moses, P. G.; Miao, M.; Yan, Q.; Van de Walle, C. G. Hybrid Functional Investigations of Band Gaps and Band Alignments for AlN, GaN, InN, and InGaN. *J. Chem. Phys.* **2011**, *134*, 084703-1−084703-11.
(50) Hummer, K.; Harl, J.; Kresse, G. Heyd-Scuseria-Ernzerhof Hybrid Functional for Calculating the Lattice Dynamics of Semiconductors. *Phys. Rev. B* **2009**, *80*, 115205-1−115205-12.
(51) Bernardi, M.; Palummo, M.; Grossman, J. C. Semiconducting Monolayer Materials as a Tunable Platform for Excitonic Solar Cells. *ACS Nano* **2012**, *6*, 10082−10089.
(52) Scharber, M. C.; Mühlbacher, D.; Koppe, M.; Denk, P.; Waldauf, C.; Heeger, A. J.; Brabec, C. J. Design Rules for Donors in Bulk-Heterojunction Solar Cells—Towards 10% Energy-Conversion Efficiency. *Adv. Mater.* **2006**, *18*, 789−794.
(53) Dai, J.; Zeng, X. C. Bilayer Phosphorene: Effect of Stacking Order on Bandgap and Its Potential Applications in Thin-Film Solar Cells. *J. Phys. Chem. Lett.* **2014**, *5*, 1289−1293.
(54) Rogal, J.; Reuter, K.; Scheffler, M. Thermodynamic Stability of PdO Surfaces. *Phys. Rev. B* **2004**, *69*, 075421-1−075421-8.
(55) Wang, Y.; Liu, H.; Lv, J.; Zhu, L.; Wang, H.; Ma, Y. High Pressure Partially Ionic Phase of Water Ice. *Nat. Commun.* **2011**, *2*, 563-1−563-5.
(56) Wang, H.; John, S. T.; Tanaka, K.; Iitaka, T.; Ma, Y. Superconductive Sodalite-like Clathrate Calcium Hydride at High Pressures. *Proc. Nat. Acad. Sci.* **2012**, *109*, 6463−6466.
(57) Xiang, H.; Huang, B.; Li, Z.; Wei, S.-H.; Yang, J.; Gong, X. Ordered Semiconducting Nitrogen-Graphene Alloys. *Phys. Rev. X* **2012**, *2*, 011003-1−011003-7.
(58) Zhu, L.; Wang, Z.; Wang, Y.; Zou, G.; Mao, H.-k.; Ma, Y. Spiral Chain O4 Form of Dense Oxygen. *Proc. Nat. Acad. Sci.* **2012**, *109*, 751−753.
(59) Dai, J.; Wu, X.; Yang, J.; Zeng, X. C. Unusual Metallic Micro-Porous Boron Nitride Networks. *J. Phys. Chem. Lett.* **2013**, *4*, 3484−3488.
(60) Li, Q.; Zhou, D.; Zheng, W.; Ma, Y.; Chen, C. Global Structural Optimization of Tungsten Borides. *Phys. Rev. Lett.* **2013**, *110*, 136403-1−136403-5.
(61) Dai, J.; Wu, X.; Yang, J.; Zeng, X. C. Porous Boron Nitride with Tunable Pore Size. *J. Phys. Chem. Lett.* **2014**, *5*, 393.
(62) Kresse, G.; Furthmüller, J. Efficient Iterative Schemes for Ab Initio Total-Energy Calculations Using a Plane-Wave Basis Set. *Phys. Rev. B* **1996**, *54*, 11169−11186.
(63) Kresse, G.; Furthmüller, J. Efficiency of Ab-initio Total Energy Calculations for Metals and Semiconductors Using a Plane-Wave Basis Set. *Comput. Mater. Sci.* **1996**, *6*, 15−50.
(64) Blöchl, P. E. Projector Augmented-Wave Method. *Phys. Rev. B* **1994**, *50*, 17953−17979.
(65) Monkhorst, H. J.; Pack, J. D. Special Points for Brillouin-Zone Integrations. *Phys. Rev. B* **1976**, *13*, 5188−5192.